Available online at www.sciencedirect.com
ScienceDirect
Electrochimica Acta 52 (2007) 2453–2460
ELECTROCHIMICA Acta
www.elsevier.com/locate/electacta

A novel approach to explore Zn based anodes for lithium-ion battery applications

N. Jayaprakash [a], K. Sathiyanarayanan [b], N. Kalaiselvi [a,*]

[a] *Central Electrochemical Research Institute, Karaikudi, India*
[b] *Vellore Institute of Technology, Vellore, India*

Received 27 June 2006; received in revised form 17 August 2006; accepted 26 August 2006
Available online 9 October 2006

Abstract

As an approach to investigate upon the electrochemical property of Zn as a possible lithium battery anode material, an ever first attempt to explore two types of Zn based alloy anodes, viz., $Zn_{0.9}Ni_{0.075}In_{0.025}$ (nickel rich) and $Zn_{0.9}Ni_{0.025}In_{0.075}$ (indium rich) was made. Citric acid assisted modified sol–gel method [CAM sol–gel] has been adopted to synthesize the anode materials at 500 °C and characterized further by XRD and SEM for phase purity and preferred surface morphology, respectively. An average crystallite size of 800 nm–1.2 μm has been calculated from the PXRD pattern and the compounds were found to exist in the cubic phase. A discharge capacity of 936 and 1155 mAh/g were exhibited by $Zn_{0.9}Ni_{0.075}In_{0.025}$ and $Zn_{0.9}Ni_{0.025}In_{0.075}$ anodes respectively, with an excellent capacity retention (>85%) and enhanced coulombic efficiency (95–98%). It is further understood that the $Zn_{0.9}Ni_{0.025}In_{0.075}$ anode with increased In content has exhibited promising electrochemical property with a steady state reversible capacity of ∼490 mAh/g even after 25 cycles, compared to the corresponding nickel rich counterpart, viz., $Zn_{0.9}Ni_{0.075}In_{0.025}$.

Keywords: Zinc alloy anodes; CAM sol–gel method; Lithium-ion battery; XRD; Specific capacity

1. Introduction

Lithium batteries are the key components of portable, entertainment and telecommunication equipments required by today's information rich e-society. The role and the demand for lithium batteries in the so-called 3C related electronic devices expand on hourly basis, irrespective of the practical difficulties encountered in deploying them as candidates of energy conversion. Despite the high irreversible capacity [1], swelling behavior or failure of the electrode through intercalation of PC based electrolyte [2], carbonaceous materials hold the major share as negative electrodes in lithium-ion batteries, since 1985. On the other hand, the outcome of several other alternate anode candidates such as metal oxides [3–5], metal phosphides [6–10] and metal vanadates [11–12] pose different types of hampering issues against their commercial exploitation. Generally, the very high irreversible capacity loss of M–M alloys (>50%) in the first cycle and deep capacity fade (∼40%) in the consecutive cycles due to exorbitant volume expansion, etc., make the compounds un suitable for global acceptance and practical lithium-ion battery applications [13]. Ultimately, the unavoidable and the unacceptable shortcomings of the individual anodes of the existing category have emphasized the need to identify novel anode candidates with comparable or better electrochemical properties than carbon.

With a view to cater to the needs and to address the shortcomings of the lithium battery technology, off late, newer metallic alloys [14], intermetallic compounds [15] and composites [16–17] are emerging as possible lithium battery anode materials. Here again, in an approach to alleviate the problems related to alloy expansion, Thackeray and co-workers proposed the selection of inter metallic anodes such as Cu_6Sn_5, Cu_2Sb and InSb, which show strong structural relationship [18] with their respective lithiated products, viz., Li_2CuSn, and LiSb. Despite the fact that, InSb and Cu_2Sb provide reversible capacities between 250 and 300 mAh/g [19], they are found to suffer from poor cyclability, particularly upon the initial cycle.

On the other hand, it is well known that zinc metal reacts with lithium reversibly to produce a maximum alloy composition of LiZn [20]. Apart from the familiarity as a battery active

* Corresponding author. Tel.: +91 4565 227550–559; fax: +91 4565 227779.
E-mail address: kalakanth2@yahoo.com (N. Kalaiselvi).

0013-4686/$ – see front matter © 2006 Elsevier Ltd. All rights reserved.
doi:10.1016/j.electacta.2006.08.071

material, Zn is known for its high dissolution and the subsequent dendrite formation, which impinges on the battery performance and extended cycle life [21]. So, with a view to exploit the maximum possible electrochemical performance of Zn as a potential lithium battery anode active material, it is believed that alloying of Zn with an inactive metal element (e.g., Ni, Fe and In) would minimize the dissolution of the same to some extent. With this background and based on our earlier report [22], that $Zn_{0.9}Ni_{0.075}In_{0.025}$ and $Zn_{0.9}Ni_{0.025}In_{0.075}$ alloy anodes are effective in enhancing the electrochemical property of Zn/air system, it is decided to synthesize the same set of anodes for the present study in order to explore and to examine the possibility of improving the electrochemical properties significantly with acceptable capacity retention, when deployed in lithium-ion batteries.

Generally, solid-state carbonate fusion method, via ball milling is adopted widely to prepare alloy anodes, wherein particle agglomeration at high sintering temperatures becomes unavoidable [23]. On the other hand, a novel CAM sol–gel method has been employed in the present study with an aim to bring down the size as well as the sintering temperature of the particles and to have the atomic level and uniform distribution of dopant metal counterparts (Ni and In) in order to ensure better homogeneity with the Zn core metal. It is further believed that the inherent high capacity of Ni and the reported enhanced structural stability of In would impart certain desirable surface modifications to the native Zn matrix as synergistic effect in the tailor-made Zn alloy anodes of $Zn_{0.9}Ni_{0.075}In_{0.025}$ and $Zn_{0.9}Ni_{0.025}In_{0.075}$ type. Similarly, the impact of CAM sol–gel methodology is expected to render better physical and electrochemical properties of the chosen category $Zn_{0.9}Ni_{0.075}In_{0.025}$ and $Zn_{0.9}Ni_{0.025}In_{0.075}$ anodes, via size driven and morphology dependent electrode characteristics. Therefore, the synthesized anode materials were examined initially through PXRD and SEM and charge–discharge studies against lithium metal finally.

2. Experimental

2.1. Synthesis procedure

The $Zn_{0.9}Ni_{0.075}In_{0.025}$ and $Zn_{0.9}Ni_{0.025}In_{0.075}$ active materials were synthesized by adopting Citric acid Assisted Modified sol–gel [CAM sol–gel] method, which is schematically represented in Fig. 1. The reaction proceeds in an acidic environment created by the addition of an organic acid. Stoichiometric proportion of high purity transition metal acetates, viz., $Zn(CH_3COO)_2$, $Ni(CH_3COO)_2$ and $In(CH_3COO)_3$ (Sigma–Aldrich, India) were dissolved in triple distilled water. The contents in the beaker were allowed to cook until fumes and a calculated quantity of citric acid was added as a complexing agent followed by the addition of acryl amide and *N*′,*N*-methylene-bis-acryl amide. Here, both the acryl amide and *N*′,*N*-methylene-bis-acryl amide act as gelling agents, whereas, citric acid with a molecular formula of $C_6H_8O_7{\cdot}H_2O$ acts as the fuel for the formation of bond between the transition metal ions and Indium [24]. Originally the carboxylic acid group that is present in the complexing agent forms a chemical bond with

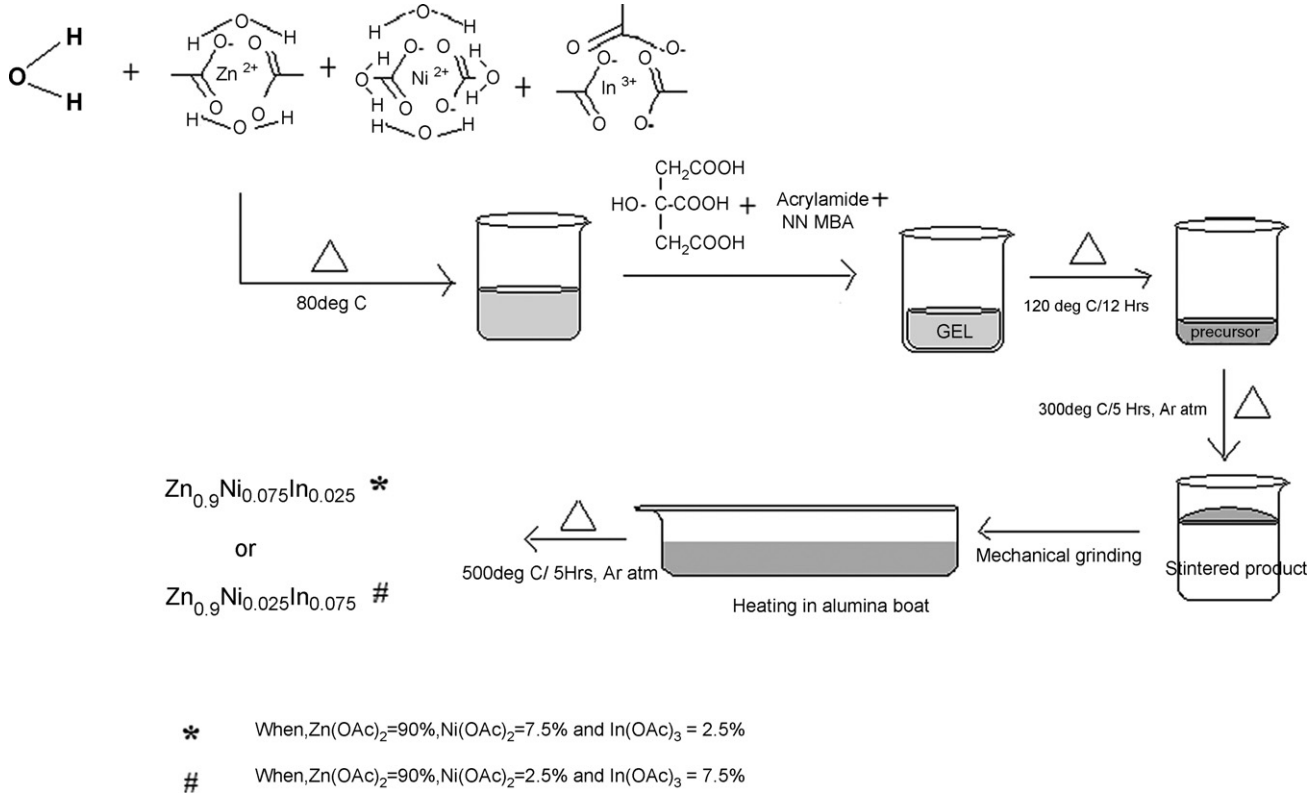

Fig. 1. Schematic representation of synthesis of $Zn_{0.9}Ni_{0.075}In_{0.025}$ and $Zn_{0.9}Ni_{0.025}In_{0.075}$, via CAM sol–gel method.

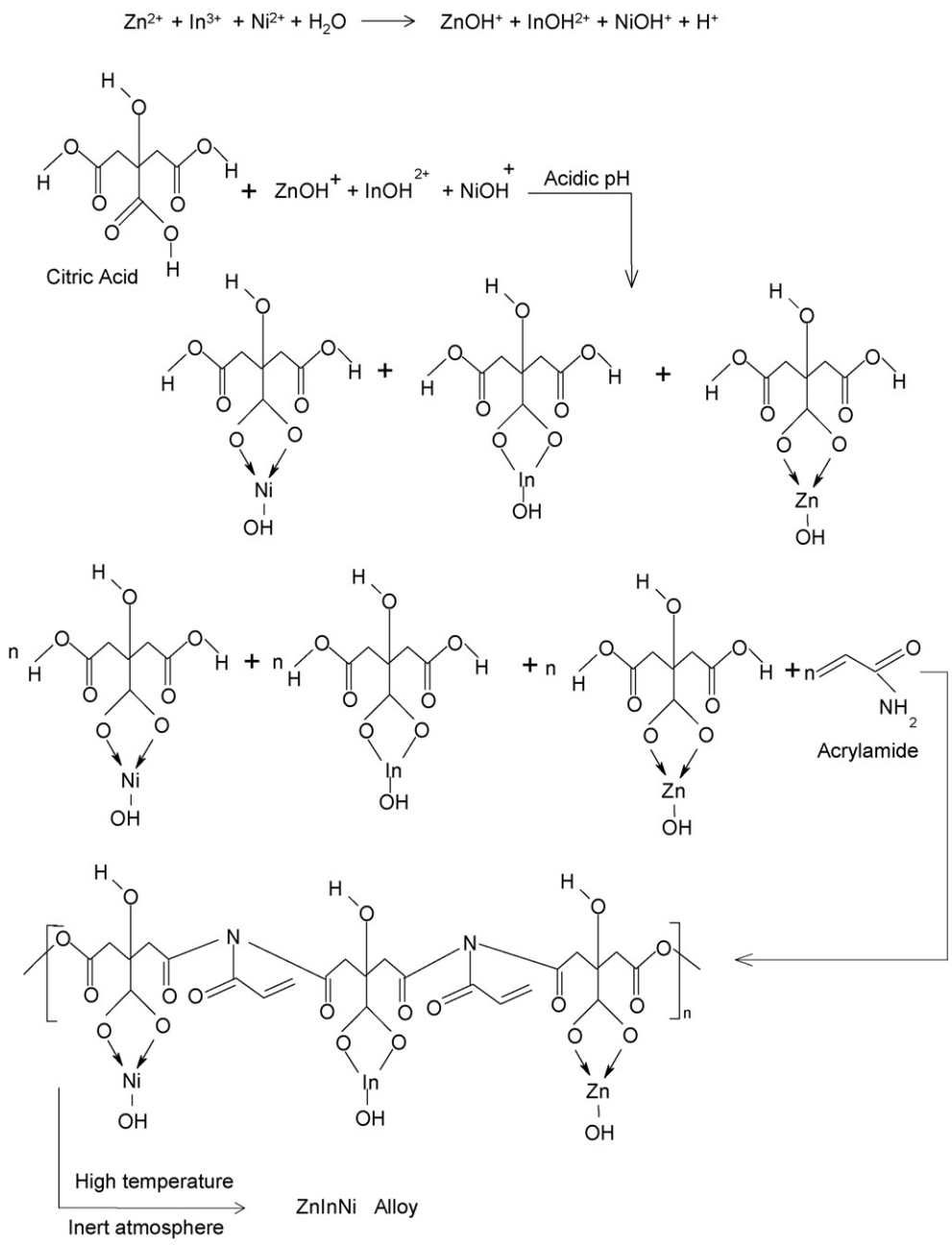

Fig. 2. Chemical reaction involved in the synthesis of Zn–Ni–In alloy.

the metal ions (Fig. 2), which upon evaporation of solvent leads to the formation of viscous resin like paste precursor [24]. It is presumed that the metal ions are trapped inside the so-called viscous resin like paste to ensure a molecular level mixing, which is the key point of the CAM sol–gel method.

2.2. Thermal treatment

The gel obtained initially, after the addition of the gelling agent, was heat treated at 120 °C for 12 h followed by sintering at 300 °C in an Ar atmosphere for about 5 h. The sintered precursor obtained in this stage was ground to yield finer particles and was further heat treated at an ambient temperature of 500 °C in the Ar atmosphere using an alumina heating boat. Here again, both the rate of heating and cooling were maintained at 1 °C/min to avoid surface cracking of the particles. Also it is noteworthy that drastic weight loss has taken place during the course of heat treatment of the precursors. The weight loss in the temperature range of 25–200 °C is due to the desorption of water, while the weight loss due to the removal of citric acid and acryl amide was observed in the temperature range of 200–300 °C [24]. Similarly the final weight loss in the temperature range of 300–500 °C may be attributed to the decomposition of metal acetates and traces of other organic substances. The complete reaction taking place during the synthesis mechanism, in the form of a reaction equation, is predicted in Fig. 2.

2.3. Physical and electrochemical characterization

Phase characterization was done by powder X-ray diffraction technique on a Philips 1830 X-ray diffractometer using Ni filtered Cu Kα radiation (λ = 1.5406) in the 2θ range of 10–120° at a scan rate of 0.04°/s. Surface morphology of the particles was examined through SEM images obtained from Jeol S-300 H Scanning Electron Microscope and the actual size of the particles was measured using Malvern easy particle size analyzer. Charge discharge studies were carried out using MACCOR charge–discharge cycler.

2.4. Electrode preparation and coin cell fabrication

Electrochemical charge–discharge evaluation was done on 2016 coin cells fabricated using the synthesized anodes and Li metal. The details pertinent to the preparation of electrodes and coin cell assembly have already been mentioned elsewhere [25].

3. Results and discussion

3.1. Phase formation results: XRD analysis

X-ray diffraction pattern of the two different alloys, viz., $Zn_{0.9}Ni_{0.075}In_{0.025}$ and $Zn_{0.9}Ni_{0.025}In_{0.075}$, synthesized at 500 °C is shown in Fig. 3a and b. The powders sintered at 500 °C exhibited well-defined Bragg peaks with preferred intensity, which is an indication that CAM sol–gel method has yielded finer powders of $Zn_{0.9}Ni_{0.075}In_{0.025}$ and $Zn_{0.9}Ni_{0.025}In_{0.075}$ with high degree of phase purity at a moderate temperature. Besides, the absence of undesirable peaks due to the formation of corresponding metal oxides or due to traces of un reacted starting materials ensure the phase purity of both the Zn based alloy compounds, which is one of the essential properties for better anode characteristics. Subsequently, the observed XRD peaks of the compounds were indexed for a cubic structure, which showed a perfect matching with the standard JCPDS values (01-1244).

The XRD pattern of $Zn_{0.9}Ni_{0.075}In_{0.025}$ and $Zn_{0.9}Ni_{0.025}In_{0.075}$ alloys contain Bragg peaks around 2θ = 31.5°, 34.5° and 36.2° that correspond to Zn (according to the standard JCPDS no. 01 1244 & 01 1238), along with the presence of peaks due to Ni (2θ = 56.8°, 70% peak of Ni as per standard JCPDS no. 01-1272) and In (2θ = 29.49°, 30% peak of In as per standard JCPDS no. 01-1042) (Fig. 3a and b), thus confirming the presence of $Zn_{0.9}Ni_{0.075}In_{0.025}$ and $Zn_{0.9}Ni_{0.025}In_{0.075}$ individually. Further, peaks at 2θ = 30.5°, 33.6° and 47.2° corresponding to the presence of respective metal oxides viz., NiO, ZnO and In_2O_3 are found to be absent, thereby confirming the exclusion of possible presence of expected oxide counterparts [22]. Hence it is believed that the compounds synthesized through the present study under the influence of Ar atmosphere have resulted in the formation of $Zn_{0.9}Ni_{0.075}In_{0.025}$ and $Zn_{0.9}Ni_{0.025}In_{0.075}$ alloys in their pure form. It is noteworthy that the 70% peak of Ni (2θ = 56.8°) and 30% peak of In (2θ = 29.49°) are only observed (rather than the respective 100% peaks), which may be due to the restricted and reduced composition of Ni and In counterparts present in the $Zn_{0.9}Ni_{0.075}In_{0.025}$ and $Zn_{0.9}Ni_{0.025}In_{0.075}$ alloys.

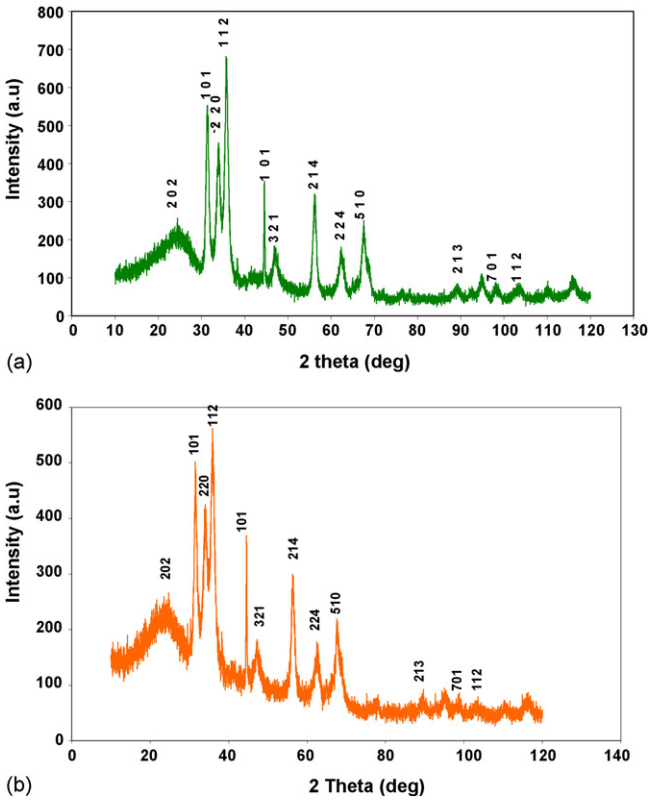

Fig. 3. XRD pattern of (a) $Zn_{0.9}Ni_{0.075}In_{0.025}$ and (b) $Zn_{0.9}Ni_{0.025}In_{0.075}$.

The lattice constant values of $Zn_{0.9}Ni_{0.075}In_{0.025}$ and $Zn_{0.9}Ni_{0.025}In_{0.075}$ [$a = b = c = 6.13$ Å] synthesized at 500 °C are in support of the fact that the Ni and In dopants have enhanced the lattice constant values [irrespective of the amount of dopants] of bare zinc [$a = 2.659$ and $c = 4.935$] (JCPDS no. 01-1238) in the tetragonal phase. This in turn is an indication that the dopants have been incorporated in to the crystal lattice of parent Zn matrix. The calculated lattice parameter values and the related physical properties are summarized in Table 1.

Generally, it is presumed that broadening of Bragg peaks originates either due to amorphicity or due to the nano-sized particles of the synthesized materials. In the present study, the observed peak broadening does not correspond to the amorphous nature of the alloy compounds, because the presence of characteristic and intense peaks could be attributed to the crystallinity

Table 1
Physical parameters of $Zn_{0.9}Ni_{0.075}In_{0.025}$ and $Zn_{0.9}Ni_{0.025}In_{0.075}$ derived from CAM sol–gel process

Compound	Lattice constant a (Å)	Cell volume (Å^3)	FWHM	Crystallite size (μm)	Stokes strain (ε_{Strain})
$Zn_{0.9}Ni_{0.075}In_{0.025}$	6.13	230.34	1.06	1.3748	0.8192
$Zn_{0.9}Ni_{0.025}In_{0.075}$	6.13	230.34	1.62	0.8997	1.2501

of the sample, as evident from Fig. 3. Therefore, it is deduced that the slightly broadened Bragg peaks of the compounds under investigation are due to the possible presence of nano-particles or nano-crystallites, which was further examined by the average crystallite size (D) calculations of the compounds. From the full width at half maximum (FWHM) values of the peaks, the average crystallite size (D) was calculated to be $\leq$1 μm using the Scherrer formula:

$$D = \frac{0.9\lambda}{\beta \cos\theta}$$

where λ is the X-ray wavelength (Å), θ the Bragg angle (in rad) and β is the FWHM (in rad, values corrected for instrumental line broadening) and the values are furnished in Table 1.

It is well known that Scherrer's calculation does not take in to consideration of the lattice strain and so, it was decided to calculate the Stoke's strain independently, in order to understand the effect of crystallite size and lattice strain on the synthesized powders separately. Because, it is also reported that apart from the finite crystallite size, peak broadening may be correlated to instrumental effects and atomic deformation from ideal position in a non uniform manner which is usually called as the strain that becomes extended defects [26] in certain cases. However, in the present study, it is understood that the peak broadening is due to the finite crystallite size and not due to the instrumental effect or strain, based on the smaller Stoke's strain values calculated using the following formula:

$$\varepsilon_{\text{Strain}} = \frac{\beta}{4\tan\theta}$$

where $\varepsilon_{\text{Strain}}$ is the weighted average strain and β is the integral breadth of a reflection (in radians 2θ) located at 2θ. The calculated strain values are found to be very small (<1.5) and based on the same, it is further substantiated that the $Zn_{0.9}Ni_{0.075}In_{0.025}$ and $Zn_{0.9}Ni_{0.025}In_{0.075}$ compounds were synthesized with preferred physical properties such as purity, crystallinity, finite particle size and free from lattice strains through the present study, which is the advantage of the CAM sol–gel methodology.

3.2. Particle size and morphology study: SEM

The scanning electron microscopic [SEM] images of the synthesized, $Zn_{0.9}Ni_{0.075}In_{0.025}$ and $Zn_{0.9}Ni_{0.025}In_{0.075}$ powders are depicted in Fig. 4a and b. Despite the 500 °C calcination temperature, no obvious agglomeration of alloy particles has been observed, which is an indication of size confinement of the individual particles. Presence of spherical grains with definite grain boundaries and the uniform distribution of alloy particles of $Zn_{0.9}Ni_{0.075}In_{0.025}$ and $Zn_{0.9}Ni_{0.025}In_{0.075}$ powders are obvious from the captured images. The particle size of the synthesized compounds were found to present well within the desired sub-micron level (~5 μm), which is in favor of the preferred morphological characteristics of a good battery electrode [27].

The presence of uniformly distributed size reduced particles of $Zn_{0.9}Ni_{0.075}In_{0.025}$ and $Zn_{0.9}Ni_{0.025}In_{0.075}$ alloys as derived from SEM has further been confirmed through particle size analysis. It is quite interesting to note that all the 100% particles of $Zn_{0.9}Ni_{0.075}In_{0.025}$ and $Zn_{0.9}Ni_{0.025}In_{0.075}$ alloys (Fig. 5a and b) are found to get distributed well within the 1–3 μm size level, which is a favorable property to exhibit better electrochemical performance. Therefore as mentioned in the PXRD and SEM results, CAM sol–gel method adopted to synthesize the present set of alloy anodes has significant effect over the size control of $Zn_{0.9}Ni_{0.075}In_{0.025}$ and $Zn_{0.9}Ni_{0.025}In_{0.075}$ alloy powders against particle agglomeration.

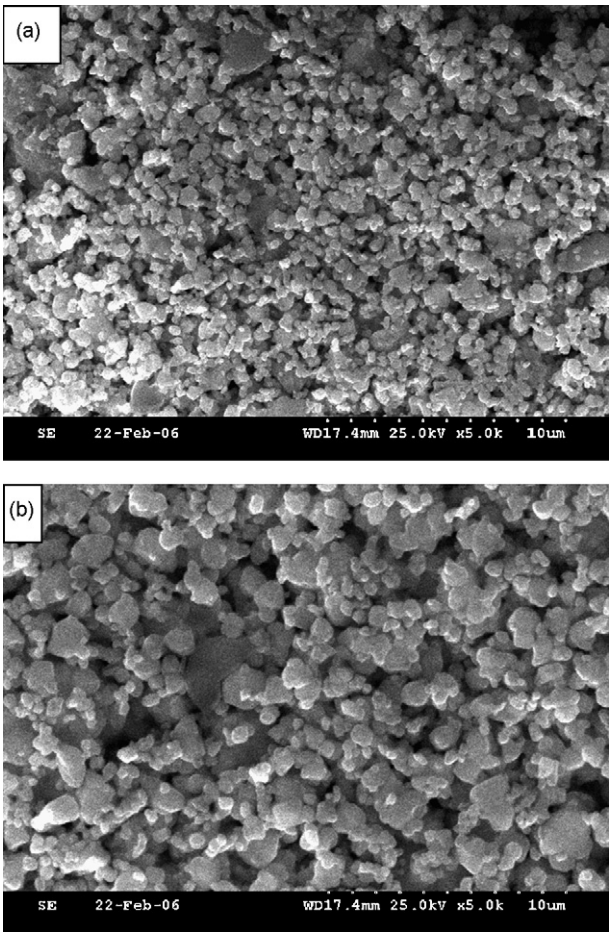

Fig. 4. Scanning electron microscopic images of (a) $Zn_{0.9}Ni_{0.075}In_{0.025}$ and (b) $Zn_{0.9}Ni_{0.025}In_{0.075}$.

3.3. Electrochemical characterization: charge–discharge studies

For better understanding, the chosen set of compounds may be classified as Ni rich ($Zn_{0.9}Ni_{0.075}In_{0.025}$) and In rich ($Zn_{0.9}Ni_{0.025}In_{0.075}$) Zn alloy anodes. The electrochemical performance of both the $Zn_{0.9}Ni_{0.075}In_{0.025}$ and $Zn_{0.9}Ni_{0.025}In_{0.075}$ alloy anodes were measured by deploying them individually as working electrodes against lithium metal counter electrode and discharging them at a constant current drain of 0.1 mA.

Basically, Zn reacts with lithium to form an alloy of LiZn composition [20] and the transformation of Zn to LiZn alloy involves several phases such as $LiZn_4$, Li_2Zn_5, $LiZn_2$ and Li_2Zn_3 [20]. However it is believed that the maximum consump-

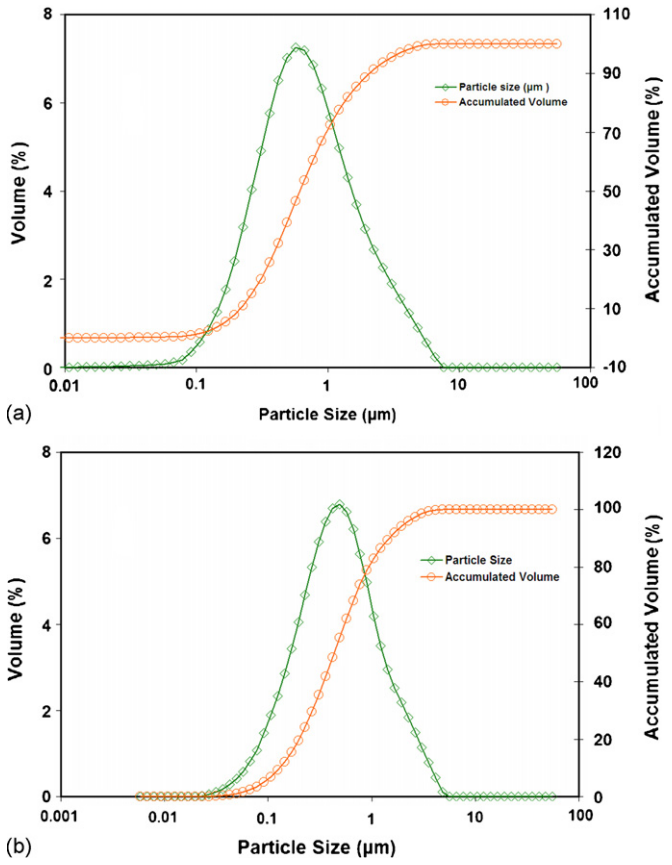

Fig. 5. Particle size distribution plot of (a) $Zn_{0.9}Ni_{0.075}In_{0.025}$ and (b) $Zn_{0.9}Ni_{0.025}In_{0.075}$.

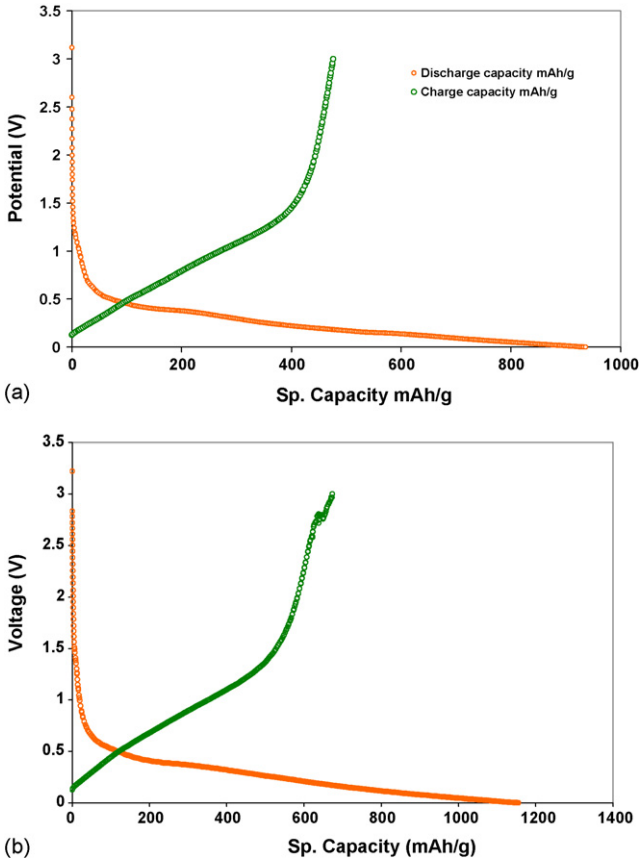

Fig. 6. Charge–discharge behavior of (a) $Zn_{0.9}Ni_{0.075}In_{0.025}$ and (b) $Zn_{0.9}Ni_{0.025}In_{0.075}$.

tion of Li in the present study would be in the range of 9–10, as inferred from the observed specific capacity values of 936 and 1155 mAh/g exhibited respectively by the Ni rich and In rich alloy anodes. Hence, capacities closer to that of theoretical value of doped alloy anodes have been realized with respect to the CAM sol–gel route $Zn_{0.9}Ni_{0.075}In_{0.025}$ and $Zn_{0.9}Ni_{0.025}In_{0.075}$ anodes, which is the highlight of the present study.

On charge, lithium is reported to get extracted initially from the LiZn alloy to form elemental Zn, as LiZn alloy is completely reversible during charge. Similarly, it is reported that partial return of original phase has been observed in the case of InSb charge [19]. Therefore, it is believed that the present study enjoys the synergistic advantages of both the Zn and In metal upon charge–discharge cycling process, especially in the case of In rich $Zn_{0.9}Ni_{0.025}In_{0.075}$. Unlike the Zn_4Sb_3 alloy [28] which is reported to show very poor electrochemical cycling life due to the destruction of the crystalline structure and fracture of grains of the alloy during insertion/extraction of Li ions, it is substantiated form the observed higher specific capacity values (>900 mAh/g) that the CAM sol–gel route wise synthesized anode materials and the electrodes prepared thereof are found to be free from surface cracks, which are responsible for volume changes during cycling. Similarly, the possible disconnection of particles upon extended cycling has also been very well managed by the meticulous and perfectly adopted electrode fabrication methods.

The initial discharge and charge curves of the $Zn_{0.9}Ni_{0.075}In_{0.025}$ and $Zn_{0.9}Ni_{0.025}In_{0.075}$ electrodes, cycled under C/10 rate are presented in Figs. 6a and b. Despite the fact that the intercalation potential may remain well below 2 V, the cells were discharged under a potential window of 0–3 V due to the intriguing interest to revisit on the intercalation behavior of Li versus $Zn_{0.9}Ni_{0.075}In_{0.025}$ and $Zn_{0.9}Ni_{0.025}In_{0.075}$ up to certain higher potential, viz., 3 V. The OCV of the $Zn_{0.9}Ni_{0.075}In_{0.025}$ and $Zn_{0.9}Ni_{0.025}In_{0.075}$ electrodes were measured to be 3.1187 and 3.2232 V versus Li/Li^+ in the delithiated state. However, upon Li^+ intercalation, the potential of the $Zn_{0.9}Ni_{0.075}In_{0.025}$ and $Zn_{0.9}Ni_{0.025}In_{0.075}$ anodes dropped quickly to 0.8 V and still lower beyond that point. In both the cases, the discharge curves show one significant plateau around 0.8 V region followed by a monotonous decrease in the voltage below 0.5 V.

Based on the observation, a discharge mechanism that involves the initial dissolution or reduction of the alloy over lithium insertion to form a lithium–metal alloy pair as experienced in the case of Zn_3P_2 system [20] may be suggested. In other words, it is presumed that lithium is extracted during charging process from the alloy–lithium pair to form the native Zn alloy and lithium in turn. Accordingly, the nickel rich $Zn_{0.9}Ni_{0.075}In_{0.025}$ alloy anode has displayed an initial discharge capacity (Q_{dc}) of 936mAh/g against a charge capacity (Q_c) of 477mAh/g i.e., an initial irreversible capacity loss of 51.5% and a coulumbic efficiency of 47.7% has been pro-

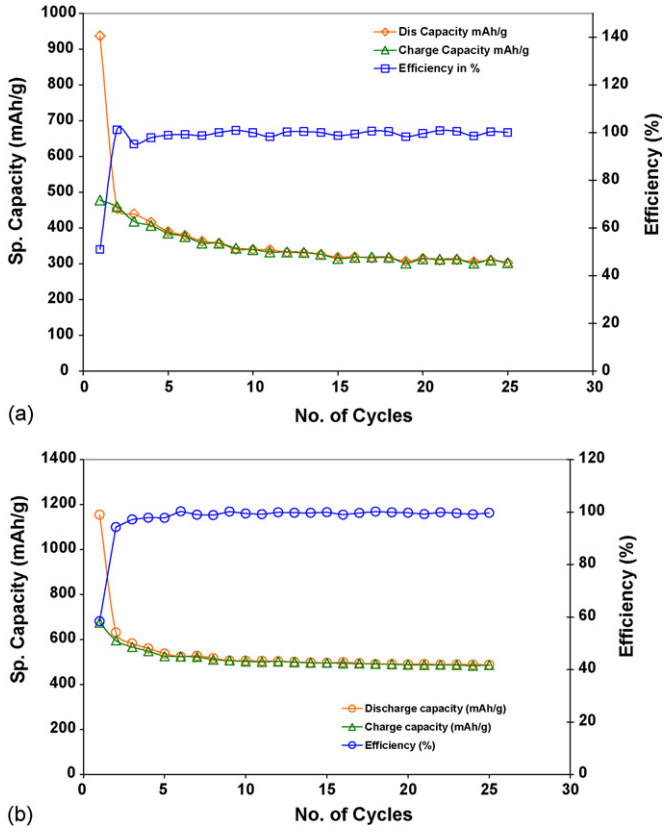

Fig. 7. Cycle life behavior of (a) $Zn_{0.9}Ni_{0.075}In_{0.025}$ and (b) $Zn_{0.9}Ni_{0.025}In_{0.075}$.

duced by the nickel rich-Zn alloy anode during the first cycle (Fig. 7a). On the other hand, during the second cycle, Q_{dc} and Q_c values of $Zn_{0.9}Ni_{0.075}In_{0.025}$ anode were found to be 454 and 459 mAh/g, respectively, corresponding to an extraordinarily enhanced coulumbic efficiency of >100%. However, a steady state anode capacity of ~350 mAh/g, a value closer to that of carbonaceous anodes [29] with a slightly varying coulumbic efficiency in the range of >90% has been observed up to 25 cycles. In other words, despite the high initial irreversible capacity values (51.5%), the observed specific capacity values of $Zn_{0.9}Ni_{0.075}In_{0.025}$ anode was found to get stabilized upon progressive cycles. Hence, it may be deduced that the nickel (rich) alloy dopant in $Zn_{0.9}Ni_{0.075}In_{0.025}$ has rendered apparent specific capacity values as that of carbon.

On the other hand, a very high initial discharge capacity of 1155 mAh/g has been exhibited by the indium rich $Zn_{0.9}Ni_{0.025}In_{0.075}$ anode with an acceptable decrease in the magnitude of reversible capacity upon cycling. Also, it is worth mentioning that the initial irreversible capacity values of the indium rich Zn alloy anode ($Zn_{0.9}Ni_{0.025}In_{0.075}$) has been minimized to an extent of 39.4% from 51.5%, as exhibited by the nickel rich $Zn_{0.9}Ni_{0.075}In_{0.025}$ anode of the present study (Fig. 7b). Thus, In rich $Zn_{0.9}Ni_{0.025}In_{0.075}$ anode showed promising electrochemical characteristics, wherein the magnitude as well as the fade in specific capacity values were modified appropriately, compared to the corresponding nickel rich $Zn_{0.9}Ni_{0.075}In_{0.025}$ alloy anode. Upon cycling, an enhanced steady state capacity values of ~490 mAh/g has been exhibited by the $Zn_{0.9}Ni_{0.025}In_{0.075}$ anode, which is higher than the specific capacity values exhibited by the commercially exploited carbonaceous and any other existing category alternative anodes [30]. Also, the coulumbic efficiency values as a function of cycle life were maintained above 98%, upon cycling without any fluctuation (Fig. 7b). In the present study, based on the observed high specific capacity values and the constantly maintained Ah efficiency values, indium rich $Zn_{0.9}Ni_{0.025}In_{0.075}$ anodes qualify themselves as superior candidates than any other anodes of the reported category. This may be attributed to the induced steric effect of In over Zn matrix, in order to impart enhanced structural stability, especially upon cycling and to some extent the enhancement may also acknowledged to the synthesis procedure adopted.

4. Conclusion

Ni rich $Zn_{0.9}Ni_{0.075}In_{0.025}$ and In rich $Zn_{0.9}Ni_{0.025}In_{0.075}$ anodes have been synthesized, via CAM sol–gel method in order to impart synergistic effects of inherent high capacity Ni and structure stabilizing In dopants. Among the two tailor-made combinations, In rich $Zn_{0.9}Ni_{0.025}In_{0.075}$ anode exhibits superior electrochemical performance in terms of high specific capacity values (~490 mAh/g) minimized irreversible capacity loss behavior (<20%) and perfectly maintained excellent coulumbic efficiency value (>98%) up to 25 cycles. On the other hand, Ni rich $Zn_{0.9}Ni_{0.075}In_{0.025}$ anode has exhibited high initial capacity values (>900 mAh/g) and comparably better reversible capacity values (~350 mAh/g) as that of carbon. Also CAM sol–gel method is found to be advantageous in producing $Zn_{0.9}Ni_{0.075}In_{0.025}$ and $Zn_{0.9}Ni_{0.025}In_{0.075}$ anode materials with finite particle size, high phase purity and better electrochemical performance.

References

[1] G.C. Chung, S.H. Jun, K.Y. Lee, M.H. Kim, J. Electrochem. Soc. 146 (1999) 1664.
[2] J. Morales, L. Sanchez, Solid State Ionics 126 (1999) 219.
[3] P. Polzot, S. Laruella, S. Grugeon, L. Dupont, J.M. Tarascon, Nature 407 (2000) 496.
[4] C.R. Sides, C.R. Martin, Adv. Mater. 17 (2005) p125.
[5] M. Hibino, K. Abe, Masafumi, Mochizuki, M. Miyayama, J. Power Sources 126 (2004) 139.
[6] D.C.S. Souza, V. Pralong, A.J. Jacobson, L.F. Nazar, Science 296 (2002) 2012.
[7] V. Pralong, D.C.S. Souza, K.T. Leung, L.F. Nazar, Electrochem. Commun. 4 (2002) 516.
[8] R. Alcántara, J.L. Tirado, J.C. Jumas, L. Monconduit, J. Olivier-Fourcade, J. Power Sources 109 (2002) 308.
[9] D.C.C. Silva, O. Crosnier, G. Ouvrard, J. Greedan, A. Safa-Sefat, L.F. Nazar, Electrochem. Solid State Lett. 6 (2003) A162.
[10] K. Wang, J. Yang, J. Xie, B. Wang, Z. Wen, Electrochem. Commun. 5 (2003) 480.
[11] Y. Idota et al. Non-aqueous battery. US patent no. 5,478,671, 1995.
[12] P. Poizot, S. Laruelle, S. Grugeon, L. Dupont, J.-M. Tarascon, Nature 407 (2000) 496.
[13] D.W. Zhang, S.Q. Zhang, Y. Jin, T.H. Yi, S. Xie, C.H. Chen, J. Alloys Compd. 415 (2006) 229.
[14] M. Nishijma, Y. Takeda, N. Imanishi, O. Yamamota, J. Solid State Chem. 113 (1994) 205.

[15] C.M. Ionica, P.E. Lippens, J.O. Fourcade, J.-C. Jumas, J. Power Sources 146 (2005) 478.
[16] J. Yang, M. Wachtler, M. Winter, J.O. Besenhard, Electrochem. Solid State Lett. 2 (1999) 161.
[17] O. Mao, J.R. Dahn, J. Electrochem. Soc. 146 (1999) 423.
[18] K.D. Kepler, J.T. Vaughey, M.M. Thackeray, Electrochem. Solid State Lett. 2 (1999) 307.
[19] T. Sarakonsri, C.S. Johnson, S.A. Hackney, M.M. Thackeray, J. Power Sources 153 (2006) 319.
[20] M.V.V.M. Satya Kishore, U.V. Varadaraju, J. Power Sources 144 (2005) 204.
[21] K. Chang Woo Lee, Sathiyanarayanan, Seung Wook Eom, Hyun Soo Kim, Mun Soo Yun, J. Power Sources 59 (2006) 1474.
[22] Chang Woo Lee, K. Sathiyanarayanan, Seung Wook Eom, Mun Soo Yun, J. Power Sources, Corrected Proof, Available online May 2, 2006, in press.
[23] G.T.-K. Fey, C.-Z. Lu, T. Prem Kumar, J. Power Sources 115 (2003) 332.
[24] C. Julian, Z. Stoynov (Eds.), Materials for Lithium-ion Batteries, Kluwer Academic Publishers, 2000, p. 549.
[25] N. Kalaiselvi, C.-H. Doh, C.-W. Park, S.-I. Moon, M.-S. Yun, Electrochem. Commun. 6 (2004) 1110.
[26] R. Jenkins, R.L. Snyder, Introduction to X-ray powder diffractometry, Wiley-Interscience, 1996.
[27] P. Kalyani, N. Kalaiselvi, N. Muniyandi, Mater. Chem. Phys. 77 (2003) 662.
[28] G.S. Cao, X.B. Zhao, T. Li, C.P. Lu, J. Power Sources 94 (2001) 102.
[29] J.R. Dahn, T. Zheng, Y. Liu, J.S. Xue, Science 270 (1995) 590.
[30] C.H. Doh, N. Kalaiselvi, C.W. Park, B.S. Jin, S.I. Moon, M.S. Yun, Electrochem. Commun. 6 (2004) 965.